Estimating FPAR of maize canopy using airborne discrete-return LiDAR data

Shezhou Luo,[1,2] Cheng Wang,[1,*] Xiaohuan Xi,[1] and Feifei Pan[3]

[1]*Key Laboratory of Digital Earth Science, Institute of Remote Sensing and Digital Earth, Chinese Academy of Sciences, Beijing 100094, China*
[2]*Beijing City University, Beijing 100083, China*
[3]*Department of Geography, University of North Texas, Denton, Texas 76203, USA*
[*]*chengwang@ceode.ac.cn*

Abstract: The fraction of absorbed photosynthetically active radiation (FPAR) is a key parameter for ecosystem modeling, crop growth monitoring and yield prediction. Ground-based FPAR measurements are time consuming and labor intensive. Remote sensing provides an alternative method to obtain repeated, rapid and inexpensive estimates of FPAR over large areas. LiDAR is an active remote sensing technology and can be used to extract accurate canopy structure parameters. A method to estimating FPAR of maize from airborne discrete-return LiDAR data was developed and tested in this study. The raw LiDAR point clouds were processed to separate ground returns from vegetation returns using a filter method over a maize field in the Heihe River Basin, northwest China. The fractional cover (fCover) of maize canopy was computed using the ratio of canopy return counts or intensity sums to the total of returns or intensities. FPAR estimation models were established based on linear regression analysis between the LiDAR-derived fCover and the field-measured FPAR (R^2 = 0.90, RMSE = 0.032, $p < 0.001$). The reliability of the constructed regression model was assessed using the leave-one-out cross-validation procedure and results show that the regression model is not overfitting the data and has a good generalization capability. Finally, 15 independent field-measured FPARs were used to evaluate accuracy of the LiDAR-predicted FPARs and results show that the LiDAR-predicted FPAR has a high accuracy (R^2 = 0.89, RMSE = 0.034). In summary, this study suggests that the airborne discrete-return LiDAR data could be adopted to accurately estimate FPAR of maize.

©2014 Optical Society of America

OCIS codes: (280.3640) Lidar; (100.6890) Three-dimensional image processing.

References and links

1. I. McCallum, W. Wagner, C. Schmullius, A. Shvidenko, M. Obersteiner, S. Fritz, and S. Nilsson, "Comparison of four global FAPAR datasets over Northern Eurasia for the year 2000," Remote Sens. Environ. **114**(5), 941–949 (2010).
2. D. Peng, B. Zhang, L. Liu, D. Chen, H. Fang, and Y. Hu, "Seasonal dynamic pattern analysis on global FPAR derived from AVHRR GIMMS NDVI," Int. J. Digit. Earth **5**(5), 439–455 (2012).
3. S. P. Serbin, D. E. Ahl, and S. T. Gower, "Spatial and temporal validation of the MODIS LAI and FPAR products across a boreal forest wildfire chronosequence," Remote Sens. Environ. **133**(0), 71–84 (2013).
4. L. Chasmer, C. Hopkinson, P. Treitz, H. McCaughey, A. Barr, and A. Black, "A liDAR-based hierarchical approach for assessing MODIS fPAR," Remote Sens. Environ. **112**(12), 4344–4357 (2008).
5. R. Fensholt, I. Sandholt, and M. S. Rasmussen, "Evaluation of MODIS LAI, fAPAR and the relation between fAPAR and NDVI in a semi-arid environment using in situ measurements," Remote Sens. Environ. **91**(3–4), 490–507 (2004).
6. N. V. Shabanov, Y. Wang, W. Buermann, J. Dong, S. Hoffman, G. R. Smith, Y. Tian, Y. Knyazikhin, and R. B. Myneni, "Effect of foliage spatial heterogeneity in the MODIS LAI and FPAR algorithm over broadleaf forests," Remote Sens. Environ. **85**(4), 410–423 (2003).
7. P. J. Sellers, C. J. Tucker, G. J. Collatz, S. O. Los, C. O. Justice, D. A. Dazlich, and D. A. Randall, "A revised

#200050 - $15.00 USD Received 25 Oct 2013; revised 18 Feb 2014; accepted 19 Feb 2014; published 26 Feb 2014
(C) 2014 OSA

land surface parameterization (SiB2) for atmospheric GCMS. part II: the generation of global fields of terrestrial biophysical parameters from satellite data," J. Clim. **9**(4), 706–737 (1996).
8. H. Lee, K. C. Slatton, B. E. Roth, and W. P. Cropper, "Prediction of forest canopy light interception using three-dimensional airborne LiDAR data," Int. J. Remote Sens. **30**(1), 189–207 (2009).
9. Q. Wang, S. Adiku, J. Tenhunen, and A. Granier, "On the relationship of NDVI with leaf area index in a deciduous forest site," Remote Sens. Environ. **94**(2), 244–255 (2005).
10. F. Chen, K. T. Weber, J. Anderson, and B. Gokhale, "Comparison of MODIS fPAR products with Landsat-5 TM-derived fPAR over semiarid Rangelands of Idaho," GISci. Remote Sens. **47**(3), 360–378 (2010).
11. J. M. Chen, J. Liu, S. G. Leblanc, R. Lacaze, and J.-L. Roujean, "Multi-angular optical remote sensing for assessing vegetation structure and carbon absorption," Remote Sens. Environ. **84**(4), 516–525 (2003).
12. D. Huang, Y. Knyazikhin, W. Wang, D. W. Deering, P. Stenberg, N. Shabanov, B. Tan, and R. B. Myneni, "Stochastic transport theory for investigating the three-dimensional canopy structure from space measurements," Remote Sens. Environ. **112**(1), 35–50 (2008).
13. R. B. Myneni, S. Hoffman, Y. Knyazikhin, J. L. Privette, J. Glassy, Y. Tian, Y. Wang, X. Song, Y. Zhang, G. R. Smith, A. Lotsch, M. Friedl, J. T. Morisette, P. Votava, R. R. Nemani, and S. W. Running, "Global products of vegetation leaf area and fraction absorbed PAR from year one of MODIS data," Remote Sens. Environ. **83**(1–2), 214–231 (2002).
14. P. Propastin and M. Kappas, "Modeling net ecosystem exchange for grassland in Central Kazakhstan by combining remote sensing and field data," Remote Sens. **1**(3), 159–183 (2009).
15. C. L. Wiegand, S. J. Maas, J. K. Aase, J. L. Hatfield, P. J. Pinter, Jr., R. D. Jackson, E. T. Kanemasu, and R. L. Lapitan, "Multisite analyses of spectral-biophysical data for wheat," Remote Sens. Environ. **42**(1), 1–21 (1992).
16. D. Van der Zande, J. Stuckens, W. W. Verstraeten, S. Mereu, B. Muys, and P. Coppin, "3D modeling of light interception in heterogeneous forest canopies using ground-based LiDAR data," Int. J. Appl. Earth Obs. Geoinf. **13**(5), 792–800 (2011).
17. M. Monsi and T. Saeki, "U¨ ber den Lichtfaktor in den Pflanzengesellschaften undseine Bedeutung fu¨ r die Stoffproduktion," Jap. J. Bot. **14**, 22–52 (1953).
18. D. Casanova, G. F. Epema, and J. Goudriaan, "Monitoring rice reflectance at field level for estimating biomass and LAI," Field Crops Res. **55**(1–2), 83–92 (1998).
19. J. L. R. Jensen, K. S. Humes, L. A. Vierling, and A. T. Hudak, "Discrete return LiDAR-based prediction of leaf area index in two conifer forests," Remote Sens. Environ. **112**(10), 3947–3957 (2008).
20. J. J. Richardson, L. M. Moskal, and S.-H. Kim, "Modeling approaches to estimate effective leaf area index from aerial discrete-return LIDAR," Agric. For. Meteorol. **149**(6–7), 1152–1160 (2009).
21. F. Baret and G. Guyot, "Potentials and limits of vegetation indices for LAI and APAR assessment," Remote Sens. Environ. **35**(2–3), 161–173 (1991).
22. J.-L. Roujean and F.-M. Breon, "Estimating PAR absorbed by vegetation from bidirectional reflectance measurements," Remote Sens. Environ. **51**(3), 375–384 (1995).
23. S. Dupuy, G. Lainé, J. Tassin, and J.-M. Sarrailh, "Characterization of the horizontal structure of the tropical forest canopy using object-based LiDAR and multispectral image analysis," Int. J. Appl. Earth Obs. Geoinf. **25**, 76–86 (2013).
24. K. C. Slatton, M. M. Crawford, and B. L. Evans, "Fusing interferometric radar and laser altimeter data to estimate surface topography and vegetation heights," IEEE Trans. Geosci. Rem. Sens. **39**(11), 2470–2482 (2001).
25. Y. Qin, T. T. Vu, Y. Ban, and Z. Niu, "Range determination for generating point clouds from airborne small footprint LiDAR waveforms," Opt. Express **20**(23), 25935–25947 (2012).
26. F. Samadzadegan, F. T. Mahmoudi, and T. Schenk, "Information fusion of Lidar range and intensity data for automatic building recognition," Int. J. Image Data Fusion **2**(1), 37–60 (2011).
27. B. D. Cook, P. V. Bolstad, E. Næsset, R. S. Anderson, S. Garrigues, J. T. Morisette, J. Nickeson, and K. J. Davis, "Using LiDAR and quickbird data to model plant production and quantify uncertainties associated with wetland detection and land cover generalizations," Remote Sens. Environ. **113**(11), 2366–2379 (2009).
28. K. Lim, P. Treitz, M. Wulder, B. St-Onge, and M. Flood, "LiDAR remote sensing of forest structure," Prog. Phys. Geogr. **27**(1), 88–106 (2003).
29. T. Hakala, J. Suomalainen, S. Kaasalainen, and Y. Chen, "Full waveform hyperspectral LiDAR for terrestrial laser scanning," Opt. Express **20**(7), 7119–7127 (2012).
30. C. Wang, M. Menenti, M. Stoll, A. Feola, E. Belluco, and M. Marani, "Separation of ground and low vegetation signatures in LiDAR measurements of salt-marsh environments," IEEE Trans. Geosci. Rem. Sens. **47**(7), 2014–2023 (2009).
31. M. A. Lefsky, A. T. Hudak, W. B. Cohen, and S. A. Acker, "Geographic variability in lidar predictions of forest stand structure in the Pacific Northwest," Remote Sens. Environ. **95**(4), 532–548 (2005).
32. F. Morsdorf, B. Kötz, E. Meier, K. I. Itten, and B. Allgöwer, "Estimation of LAI and fractional cover from small footprint airborne laser scanning data based on gap fraction," Remote Sens. Environ. **104**(1), 50–61 (2006).
33. E. Næsset, "Effects of different sensors, flying altitudes, and pulse repetition frequencies on forest canopy metrics and biophysical stand properties derived from small-footprint airborne laser data," Remote Sens. Environ. **113**(1), 148–159 (2009).
34. A. Peduzzi, R. H. Wynne, T. R. Fox, R. F. Nelson, and V. A. Thomas, "Estimating leaf area index in intensively managed pine plantations using airborne laser scanner data," For. Ecol. Manage. **270**(0), 54–65 (2012).

#200050 - $15.00 USD Received 25 Oct 2013; revised 18 Feb 2014; accepted 19 Feb 2014; published 26 Feb 2014
(C) 2014 OSA

35. S. C. Popescu, R. H. Wynne, and R. F. Nelson, "Measuring individual tree crown diameter with lidar and assessing its influence on estimating forest volume and biomass," Can. J. Rem. Sens. **29**(5), 564–577 (2003).
36. G. Sun, K. J. Ranson, Z. Guo, Z. Zhang, P. Montesano, and D. Kimes, "Forest biomass mapping from lidar and radar synergies," Remote Sens. Environ. **115**(11), 2906–2916 (2011).
37. K. Zhao and S. Popescu, "Lidar-based mapping of leaf area index and its use for validating GLOBCARBON satellite LAI product in a temperate forest of the southern USA," Remote Sens. Environ. **113**(8), 1628–1645 (2009).
38. V. Thomas, D. A. Finch, J. H. McCaughey, T. Noland, L. Rich, and P. Treitz, "Spatial modelling of the fraction of photosynthetically active radiation absorbed by a boreal mixedwood forest using a LiDAR-hyperspectral approach," Agric. For. Meteorol. **140**(1–4), 287–307 (2006).
39. K. W. Todd, F. Csillag, and P. M. Atkinson, "Three-dimensional mapping of light transmittance and foliage distribution using LiDAR," Can. J. Rem. Sens. **29**(5), 544–555 (2003).
40. C. S. T. Daughtry, K. P. Gallo, S. N. Goward, S. D. Prince, and W. P. Kustas, "Spectral estimates of absorbed radiation and phytomass production in corn and soybean canopies," Remote Sens. Environ. **39**(2), 141–152 (1992).
41. L.-C. Inc, "LI-COR Terrestrial Radiation Sensors Instruction Manual," LI–COR Inc., Lincoln, Nebraska, 1–38 (2005).
42. S. T. Gower, C. J. Kucharik, and J. M. Norman, "Direct and Indirect Estimation of Leaf Area Index, fAPAR, and Net Primary Production of Terrestrial Ecosystems," Remote Sens. Environ. **70**(1), 29–51 (1999).
43. P. Axelsson, "DEM generation from laser scanner data using adaptive tin models," Int. Arch. Photogramm. Remote Sens. **33**, 111–118 (2000).
44. C. Hopkinson and L. Chasmer, "Testing LiDAR models of fractional cover across multiple forest ecozones," Remote Sens. Environ. **113**(1), 275–288 (2009).
45. L. Korhonen, I. Korpela, J. Heiskanen, and M. Maltamo, "Airborne discrete-return LIDAR data in the estimation of vertical canopy cover, angular canopy closure and leaf area index," Remote Sens. Environ. **115**(4), 1065–1080 (2011).
46. S. Solberg, "Mapping gap fraction, LAI and defoliation using various ALS penetration variables," Int. J. Remote Sens. **31**(5), 1227–1244 (2010).
47. B. C. Bright, J. A. Hicke, and A. T. Hudak, "Estimating aboveground carbon stocks of a forest affected by mountain pine beetle in Idaho using lidar and multispectral imagery," Remote Sens. Environ. **124**, 270–281 (2012).
48. F. J. Mesas-Carrascosa, I. L. Castillejo-González, M. S. de la Orden, and A. G.-F. Porras, "Combining LiDAR intensity with aerial camera data to discriminate agricultural land uses," Comput. Electron. Agric. **84**(0), 36–46 (2012).
49. M. García, D. Riaño, E. Chuvieco, and F. M. Danson, "Estimating biomass carbon stocks for a Mediterranean forest in central Spain using LiDAR height and intensity data," Remote Sens. Environ. **114**(4), 816–830 (2010).
50. B. Höfle and N. Pfeifer, "Correction of laser scanning intensity data: Data and model-driven approaches," ISPRS J. Photogramm. Remote Sens. **62**(6), 415–433 (2007).
51. A. Kukko, S. Kaasalainen, and P. Litkey, "Effect of incidence angle on laser scanner intensity and surface data," Appl. Opt. **47**(7), 986–992 (2008).
52. M. A. Lefsky, W. B. Cohen, S. A. Acker, G. G. Parker, T. A. Spies, and D. Harding, "LiDAR remote sensing of the canopy structure and biophysical properties of douglas-fir western Hemlock forests," Remote Sens. Environ. **70**(3), 339–361 (1999).
53. S. Luo, C. Wang, G. Li, and X. Xi, "Retrieving leaf area index using ICESat/GLAS full-waveform data," Remote Sens. Lett. **4**(8), 745–753 (2013).
54. J. E. Means, S. A. Acker, D. J. Harding, J. B. Blair, M. A. Lefsky, W. B. Cohen, M. E. Harmon, and W. A. McKee, "Use of large-footprint scanning airborne LiDAR to estimate forest stand characteristics in the western Cascades of Oregon," Remote Sens. Environ. **67**(3), 298–308 (1999).
55. D. Riaño, F. Valladares, S. Condés, and E. Chuvieco, "Estimation of leaf area index and covered ground from airborne laser scanner (LiDAR) in two contrasting forests," Agric. For. Meteorol. **124**(3–4), 269–275 (2004).
56. M. A. Brovelli, M. Crespi, F. Fratarcangeli, F. Giannone, and E. Realini, "Accuracy assessment of high resolution satellite imagery orientation by leave-one-out method," ISPRS J. Photogramm. Remote Sens. **63**(4), 427–440 (2008).
57. S. Tonolli, M. Dalponte, M. Neteler, M. Rodeghiero, L. Vescovo, and D. Gianelle, "Fusion of airborne LiDAR and satellite multispectral data for the estimation of timber volume in the Southern Alps," Remote Sens. Environ. **115**(10), 2486–2498 (2011).
58. M. García, D. Riaño, E. Chuvieco, J. Salas, and F. M. Danson, "Multispectral and LiDAR data fusion for fuel type mapping using Support Vector Machine and decision rules," Remote Sens. Environ. **115**(6), 1369–1379 (2011).
59. B. Koetz, G. Sun, F. Morsdorf, K. J. Ranson, M. Kneubühler, K. Itten, and B. Allgöwer, "Fusion of imaging spectrometer and LIDAR data over combined radiative transfer models for forest canopy characterization," Remote Sens. Environ. **106**(4), 449–459 (2007).
60. T. L. Erdody and L. M. Moskal, "Fusion of LiDAR and imagery for estimating forest canopy fuels," Remote Sens. Environ. **114**(4), 725–737 (2010).
61. S. C. Popescu, R. H. Wynne, and J. A. Scrivani, "Fusion of small-footprint LiDAR and multispectral data to

#200050 - $15.00 USD Received 25 Oct 2013; revised 18 Feb 2014; accepted 19 Feb 2014; published 26 Feb 2014
(C) 2014 OSA

estimate plot-level volume and biomass in deciduous and pine forests in Virginia, USA," For. Sci. **50**(4), 551–565 (2004).
62. M. Dalponte, L. Bruzzone, and D. Gianelle, "Fusion of hyperspectral and LiDAR remote sensing data for classification of complex forest areas," IEEE Trans. Geosci. Rem. Sens. **46**(5), 1416–1427 (2008).
63. L. Ronggao, L. Shunlin, H. Honglin, L. Jiyuan, and Z. Tao, "Mapping incident photosynthetically active radiation from MODIS data over China," Remote Sens. Environ. **112**(3), 998–1009 (2008).
64. F. Morsdorf, C. Nichol, T. Malthus, and I. H. Woodhouse, "Assessing forest structural and physiological information content of multi-spectral LiDAR waveforms by radiative transfer modelling," Remote Sens. Environ. **113**(10), 2152–2163 (2009).

1. Introduction

The fraction of photosynthetically active radiation (PAR) absorbed by vegetation in the 0.4-0.7μm spectrum, also known as FPAR, is one of important terrestrial variables controlling the mass and energy exchanges between vegetation and the atmosphere [1–3], and therefore is one of key parameters required in crop production models and Earth system models for simulating land vegetation-atmosphere interactions [4–7]. FPAR can be directly measured using the traditional and accurate ground-based methods, but direct measurements of FPAR are difficult and time consuming [1, 4, 8]. In addition, it is not feasible to apply the ground-based methods to measure FPAR across large landscapes [9]. Even at some regional scales, these methods are also difficult to use to measure FPAR for studying spatial patterns of FPAR [10]. Remote sensing provides an alternative and unique method to obtain repeated, rapid and inexpensive estimates of FPAR over large areas [6, 11]. Passive remote sensing data have been widely used to derive FPAR using radiative transfer models or empirical relationships between FPAR and vegetation indices [5, 12]. Previous studies showed a linear or close linear relationship between vegetation index (VI) and FPAR [5, 13], where commonly used vegetation indices include the normalized difference vegetation index (NDVI), the simple ratio (SR), and the enhanced vegetation index (EVI). Propastin and Kappas [14] estimated FPAR of a grassland using a linear regression model between the ground-measured FPAR values and the corresponding NDVI values derived from SPOT-VGT data. Peng et al. [2] retrieved global FPAR using the FPAR-SR relationship as shown in Eq. (1) [7]:

$$FPAR = \frac{(SR - SR_{i,\min})(FPAR_{\max} - FPAR_{\min})}{SR_{i,\max} - SR_{i,\min}} + FPAR_{\min}. \quad (1)$$

where $SR = (1 + NDVI)/(1-NDVI)$, $FPAR_{\max} = 0.950$, $FPAR_{\min} = 0.001$; $FPAR_{\max}$ and $FPAR_{\min}$ are independent of vegetation type; $SR_{i,\max}$ is the SR value corresponding to 98% of $NDVI$ population for type i vegetation; $SR_{i,\min}$ is the SR value corresponding to 5% of $NDVI$ population for type i vegetation.

FPAR can also be estimated from empirical relationships between field-measured FPAR and leaf area index (LAI) [15]. Beer-Lambert law has been widely used to describe the exponential attenuation of monochromatic radiation in a canopy and approximates vegetation as a turbid medium [16, 17]. Casanova et al. [18] found the ratio between transmitted and incoming photosynthetically active radiation (PAR; 0.4-0.7μm) under a canopy decreases approximately exponentially with LAI, and thus the FPAR can be expressed as a function of LAI as follows:

$$FPAR = 1 - e^{-c \times LAI}. \quad (2)$$

where $FPAR$ is fraction of PAR intercepted by the canopy, c is extinction coefficient and LAI is leaf area index.

Although vegetation indexes can be used to estimate FPAR, accuracy in the estimated FPAR is limited by saturation of vegetation indexes, because canopy spectral reflectance is less sensitive to LAI variation as LAI is greater than 3.0 [19, 20]. The FPAR estimation based on Eq. (2) is also affected by the background spectral information if LAI is low [21, 22].

#200050 - $15.00 USD Received 25 Oct 2013; revised 18 Feb 2014; accepted 19 Feb 2014; published 26 Feb 2014
(C) 2014 OSA

Furthermore, since optical remotely sensed data do not take into account the three-dimensional structural characteristics of the canopy cover, the information reflected in the two-dimensional data such as multi-spectral imagery is not sufficient for estimating FPAR [8]. Although interferometric synthetic aperture radar (InSAR) can provide some three-dimensional vegetation structural information, the coarse spatial resolution associated with InSAR suggests that the current InSAR technique is incapable of measuring stand-scale canopy vertical structures [8, 23, 24].

LiDAR (Light Detection and Ranging) is an active remote sensing technology and has been widely used in extracting three-dimensional information of land surfaces [25, 26], such as fine spatial resolution and high vertical accuracy 3D structural characteristics of plant cover [27, 28], which are very useful for studying forest canopy structure and leaf physiology, and estimating biophysical parameters [29, 30], e.g., tree height, crown width, fractional cover, LAI, total aboveground biomass, and timber volume [e.g., 31–37]. LiDAR systems have the ability to penetrate into vegetation canopy and thus can be used to characterize light transmittance through the canopy [38, 39]. This, in turn, provides information about the available light for photosynthesis and its variation over the entire canopy depth [38].

Several studies have shown that airborne LiDAR data can be used to accurately estimate FPAR based on empirical relationships between FPAR and LiDAR derived metrics [e.g., 4, 8, 38, 39]. Recent studies that used LiDAR data to estimate FPAR tended to concentrate on forest vegetation [e.g., 8, 39], and application of LiDAR data to estimate FPAR of crops such as maize and sorghum has barely been investigated. However, FPAR is an important parameter in many crop growth and yield models [e.g., 1, 40]. Therefore, this study aimed to estimate FPAR of maize using airborne discrete-return LiDAR data. Three main objectives were pursued to achieve the goal of this study: 1) computing vegetation cover (fCover) using the ratio of canopy return counts or intensity sums to the total of returns or intensities; 2) establishing a series of regression relationships between LiDAR-derived fCover and field-measured FPAR; and 3) evaluating the reliability of the constructed regression model by performing the leave-one-out cross-validation (LOOCV) analysis and validating the accuracy of the LiDAR-predicted FPARs.

2. Materials and methods

2.1 Study area

The study area is in the Heihe River Basin, northwest China (38°56′N-38°59′N, 100°25′E-100°28′E) (Fig. 1). The mean annual air temperature, precipitation and potential evapotranspiration are about 7.3 °C, 129 mm, and 2047 mm in this arid region, respectively. The terrain in the study area is relatively flat with a mean elevation of 1403 m above sea level. A total of 40 FPAR values were measured in six sampling areas (see Fig. 1).

#200050 - $15.00 USD Received 25 Oct 2013; revised 18 Feb 2014; accepted 19 Feb 2014; published 26 Feb 2014
(C) 2014 OSA

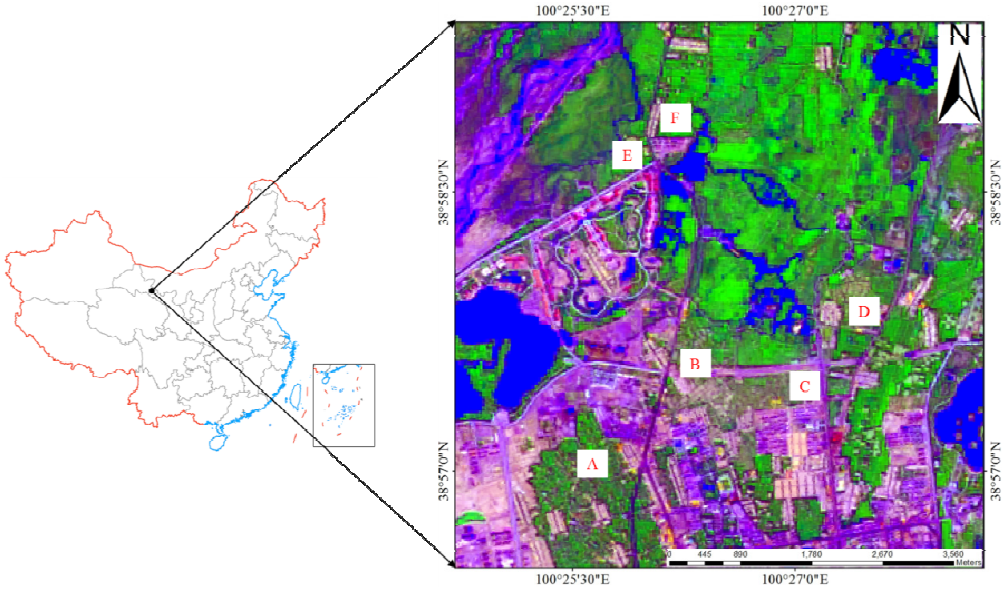

Fig. 1. The location of study area. A, B, C, D, E and F are six sampling areas where FPAR was measured using the ground-based method.

2.2 Field measurements

The field experiment was conducted in July 2012. The FPAR was measured as photosynthetic photon flux density (PPFD, μmol m^{-2} s^{-1}) using LI-191SA Linear Quantum PAR Sensor (LI-COR, Inc.) [41]. This sensor spatially averages radiation over its 1 meter length, minimizes the error and allows one person to easily make many measurements in a short period of time (LI-COR, Inc.) [41]. To obtain FPAR, above-canopy downwelling (PAR_{ad}) and upwelling (PAR_{au}) PAR, below-canopy downwelling (PAR_{bd}) and upwelling (PAR_{bu}) PAR were measured for each sample plot. Linear quantum sensor was at an approximate height of 0.5 m above the canopy surface and 0.15 m above the ground for all measurements, respectively. This placement ensured that the sensor was above the short grass vegetation in each sampling plot. To reduce the error, the sensor was kept level when all the measurements were taken. FPAR was calculated based on Eq. (3) for each plot.

$$FPAR = \frac{(PAR_{ad} - PAR_{au}) - (PAR_{bd} - PAR_{bu})}{PAR_{ad}} \tag{3}$$

where PAR_{ad} and PAR_{au} are incident and reflected PAR above the canopy, respectively; PAR_{bd} and PAR_{bu} are incident and reflected PAR below the canopy, respectively [42].

The geographic coordinates of each plot center point were measured using a centimeter-level GPS with a horizontal accuracy of 0.012 m and a vertical accuracy of 0.01 m. A total of 40 plots with an area of 5.0 m x 5.0 m each were measured at representative sites across the study area. The maize crop during the field survey was between pre-flowering and flowering stages. The average height of maize was 1.85 m, and the average row spacing and intra-row spacing were about 0.6 m and 0.25 m, respectively.

2.3 Collection of airborne LiDAR data

Small footprint airborne LiDAR data were acquired in July 2012 using a Leica ALS70 system. For the study area, the scan angle was ± 18° with a 60%)ight line side lap. The average flying height was 1300 m above the ground with a velocity of 60 m/s and an average

#200050 - $15.00 USD Received 25 Oct 2013; revised 18 Feb 2014; accepted 19 Feb 2014; published 26 Feb 2014
(C) 2014 OSA

point density of 7.4 points/m^2. Raw LiDAR data was converted to a LAS binary format file including x, y, z coordinates and intensity return values.

2.4 LiDAR data processing

The flowchart of LiDAR data processing and PFAR estimation is shown in Fig. 2. Raw airborne LiDAR data may contain some outliers, which are extremely higher or lower than other points in the vicinity and isolated points up in the air or below the ground. Outliers were removed from raw LiDAR data before they were processed by the TerraScan software (TerraSolid, Ltd., Finland). Then LiDAR point clouds were classified as canopy and ground returns using the progressive triangulated irregular network (TIN) densification method proposed by Axelsson [43] in the TerraScan software. It is very important to carry out some manual check and reclassification since the classification may misclassify some points and any misclassification of point clouds could result in significant errors in the extracted DEM and vegetation structural parameters.

The fractional cover of canopy (fCover) is defined as the fraction of ground covered by vegetation [32]. The LiDAR derived canopy fractional cover can be calculated as the ratio of the number of canopy laser returns or intensity sums to total returns or intensities based on Eq. (4) [e.g., 4, 20, 32, 44–46].

$$fCover = \frac{N_{\text{canopy}}}{N_{\text{total}}}. \tag{4}$$

where *fCover* is the fractional cover of canopy, N_{canopy} is the number of canopy laser returns or the sum of intensity and N_{total} is the total returns or intensities.

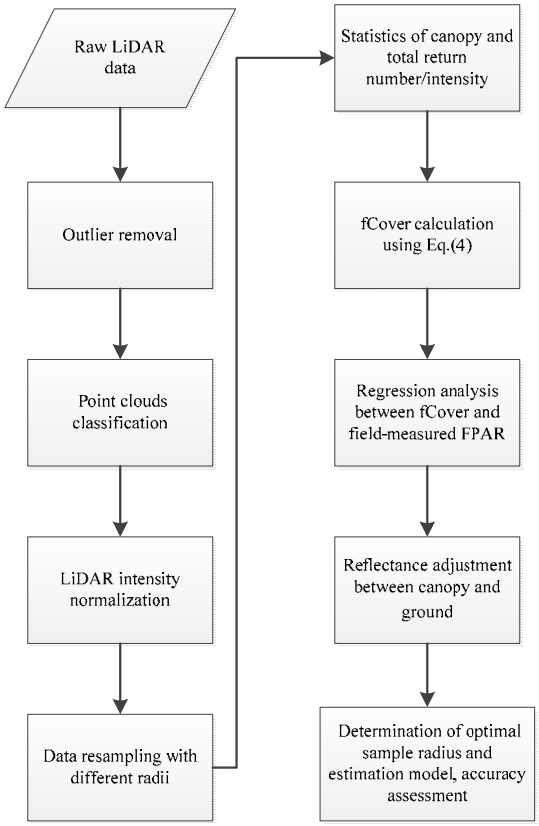

Fig. 2. Flow chart of LiDAR data processing and PFAR estimation.

#200050 - $15.00 USD Received 25 Oct 2013; revised 18 Feb 2014; accepted 19 Feb 2014; published 26 Feb 2014
(C) 2014 OSA

LiDAR intensity is the amount of energy reflected back to the LiDAR sensor, which is a function of several variables such as laser power, angle of incidence, target reflectivity and LiDAR sensor-to-target range [47, 48]. It is therefore necessary to calibrate intensity values to achieve a better comparison among different strips, flights or regions [49]. To improve accuracy of the LiDAR derived canopy fractional cover, LiDAR intensity data were normalized using Eq. (5) [50].

$$I_{\text{normalized}} = I \frac{R^2}{R_s^2 \cos\alpha}. \quad (5)$$

where $I_{\text{normalized}}$ is the normalized intensity, I is the raw intensity, R is the sensor to target range, R_s is the reference range or average flying height (in this study R_s = 1000 m) and a is the angle of incidence. Since this study area has a relatively flat terrain, the scanning angle and the angle of incidence were approximately equal. Therefore, we used the scan angle as the incidence angle a in Eq. (5), and the effect of terrain on the LiDAR intensity was neglected in this study [49, 51].

The reflectances are different between the canopy and ground at the infrared wavelength (1064 nm). To reduce the effect of this reflectance difference on accuracy in the estimated canopy fractional cover, the LiDAR intensity values of canopy and ground need be adjusted according to Eq. (6) [52–54].

$$I_{\text{canopy}} = kI_{ground}. \quad (6)$$

where k is the adjusting factor of reflectance, I_{canopy} and I_{ground} are the intensity of canopy and ground, respectively. In this regard, previous studies generally used 2.0 as the k value in calculating *fCover* [e.g., 52–54]. To determine the optimal k value and improve the accuracy of FPAR estimation, we examined a sequence of k values from 1.0 m to 10.0 m with an increment of 0.5 m and selected the value that yielded the highest R^2 value in a linear regression against the field-measured FPAR [46].

2.5 FPAR estimation from LiDAR data

The *fCover* is dependent on canopy structure up to a certain radius size and the trial-and-error method could be used to determine an optimal radius size [55]. Previous studies provided experiential evidence on how to identify a reasonable radius size [32, 37]. To obtain the optimal plot size for estimating FPAR from the LiDAR data, the center coordinates of each plot were applied to extract return counts and intensity for each plot with different radii from classified LiDAR point clouds. We examined a range of plot radii from 1.0 m to 7.0 m with an increment of 0.5 m. For each plot, the number of canopy returns and the sum of intensity (N_{canopy}) and the total returns and intensities (N_{total}) were calculated for each specific radius. LiDAR return- and intensity-based *fCover* of each plot were computed according to Eq. (4) using N_{canopy} and N_{total}, respectively. The linear regression analysis of the LiDAR-derived *fCover* against the field-measured FPAR was carried out to build an empirical FPAR estimation model as given in Eq. (7):

$$y = ax + b \quad (7)$$

where y is FPAR, x is *fCover* based on returns or intensities, a and b are the slope and the y intercept of the regression line, respectively. The coefficient of determination (R^2), the adjusted R^2 (adj. R^2) and the root mean square error (RMSE) across a range of plot sizes (i.e., 1.0 m-7.0 m in radius) were calculated. The statistical results of each radius were compared for determining the optimal FPAR estimation model and the optimal plot size.

#200050 - $15.00 USD Received 25 Oct 2013; revised 18 Feb 2014; accepted 19 Feb 2014; published 26 Feb 2014
(C) 2014 OSA

3. Results and validation

3.1 Results

Since *fCover* varies with the plot size [37, 55], to investigate the effect of different plot sizes on model performance, *fCover* was estimated on the 40 field plots using a range of plot radii from 1.0 m to 7.0 m with an increment of 0.5 m. A linear regression analysis (i.e., Eq. (7)) between 25 field-measured FPARs and LiDAR-derived *fCover* values was carried out. The statistical characteristics of the estimated FPARs with different plot radius are shown in Table 1. According to Table 1, as the plot radius is 4.0 m, both LiDAR return- and intensity-based *fCover* estimations have the smallest RMSE and the highest correlation with the field-measured FPAR.

Table 1. Statistical characteristics of estimated fpars with different sample radii

Plot radii (m)	Based on LiDAR return count			Based on LiDAR intensity		
	R^2	Adj.R^2	RMSE	R^2	Adj.R^2	RMSE
1.0	0.23	0.19	0.088	0.22	0.19	0.088
1.5	0.26	0.23	0.086	0.32	0.29	0.082
2.0	0.32	0.30	0.082	0.44	0.42	0.075
2.5	0.60	0.58	0.063	0.63	0.61	0.060
3.0	0.77	0.76	0.047	0.80	0.79	0.044
3.5	0.83	0.82	0.042	0.85	0.84	0.037
4.0	0.85	0.84	0.038	0.86	0.86	0.036
4.5	0.84	0.83	0.039	0.85	0.84	0.038
5.0	0.82	0.81	0.043	0.83	0.82	0.041
5.5	0.80	0.79	0.045	0.82	0.81	0.042
6.0	0.78	0.77	0.048	0.76	0.75	0.049
6.5	0.75	0.74	0.050	0.74	0.73	0.050
7.0	0.72	0.71	0.053	0.73	0.72	0.051

Accounting for the reflectance difference between the canopy and ground, the *fCover* was calculated using Eq. (8) to improve the accuracy of FPAR estimation.

$$fCover = \frac{N_{\text{canopy}}}{N_{\text{total}}} = \frac{N_{\text{canopy}}}{N_{\text{canopy}} + kN_{\text{ground}}} \tag{8}$$

where N_{ground} is the sum of ground laser return intensity. We adjusted the intensity of a plot of radius 4.0 m using a sequence of k values from 1.0 m to 10.0 m with an increment of 0.5 m. Results showed the accuracy of intensity-based FPAR estimation was the highest ($R^2 = 0.90$) as the k value was 3.0 in Eq. (8), while R^2 was 0.85 for the LiDAR return-based *fCover* estimation. Scatterplots of the LiDAR-derived *fCover* versus the field-measured FPAR and the corresponding regression models are presented in Fig. 3.

#200050 - $15.00 USD Received 25 Oct 2013; revised 18 Feb 2014; accepted 19 Feb 2014; published 26 Feb 2014
(C) 2014 OSA

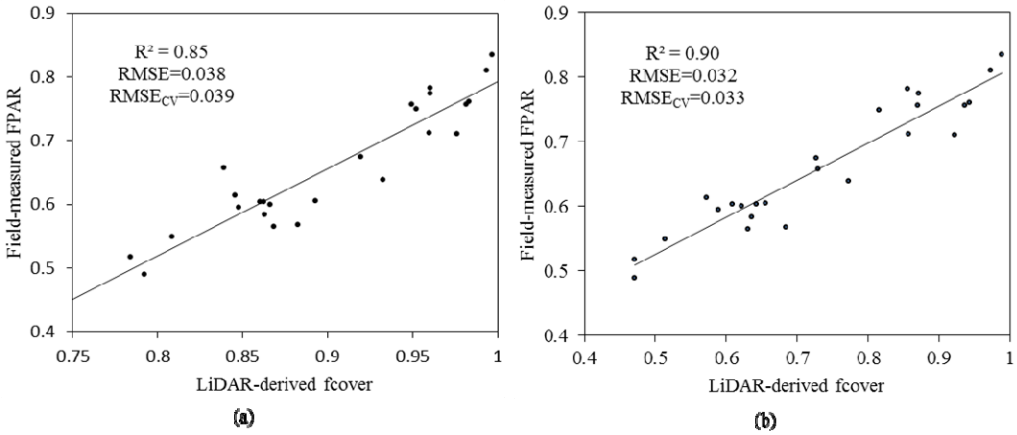

Fig. 3. (a) Scatterplot of the return-based LiDAR-derived fCover versus the field-measured FPAR and the corresponding regression model (R2 = 0.85, RMSE = 0.038, n = 25, p<0.001). (b) Scatterplot of the intensity-based LiDAR-derived fCover versus the field-measured FPAR and the corresponding regression model (R2 = 0.90, RMSE = 0.032, n = 25, p<0.001).

To determine the optimal model of FPAR estimation using the airborne LiDAR data, we compared the LiDAR intensity-based and return-based models. Results indicate that the intensity-based prediction model had the highest accuracy (R^2 = 0.90, *adj.* R^2 = 0.89, RMSE = 0.032) and yielded slightly better estimates compared to the LiDAR return-based model (R^2 = 0.85, *adj.* R^2 = 0.84, RMSE = 0.038). This result is in a good agreement with Hopkinson and Chasmer's results which showed that laser intensity can potentially provide an accurate estimate of FPAR [44], because the intensity methods implicitly provide some quantification of the surface area that the pulse is interacting with in the form of the reflectance amplitude (e.g., intensity) [44].

3.2 Accuracy assessment

To assess the model's reliability, the predicted residual sums of squares (PRESS statistic) was calculated using the leave-one-out cross-validation (LOOCV) analysis [37, 56], which is an effective method to evaluate the generalization capability of regression models, being particularly useful when a low number of field-measured data are available [56]. The root mean square error from the cross validation analysis ($RMSE_{cv}$) was computed as the square root of the ratio between the PRESS statistic and the number of observations [34]. The $RMSE_{cv}$ was 0.033 for the intensity-based regression model and the RMSE was 0.032. The close consistency between the $RMSE_{cv}$ and the RMSE suggests that the regression model is not overfitting the data and has a good generalization capability. In addition, we obtained the accuracy of LiDAR-predicted FPARs using other 15 field-measured FPARs which are not used for the regression analysis (Twenty-five out of the total 40 field-measured FPARs were used to construct the FPAR estimation model). Results show a good relationship (R^2 = 0.89, RMSE = 0.034, $RMSE_{cv}$ = 0.035) between the field-measured and the LiDAR-predicted FPARs (Fig. 4).

#200050 - $15.00 USD Received 25 Oct 2013; revised 18 Feb 2014; accepted 19 Feb 2014; published 26 Feb 2014
(C) 2014 OSA

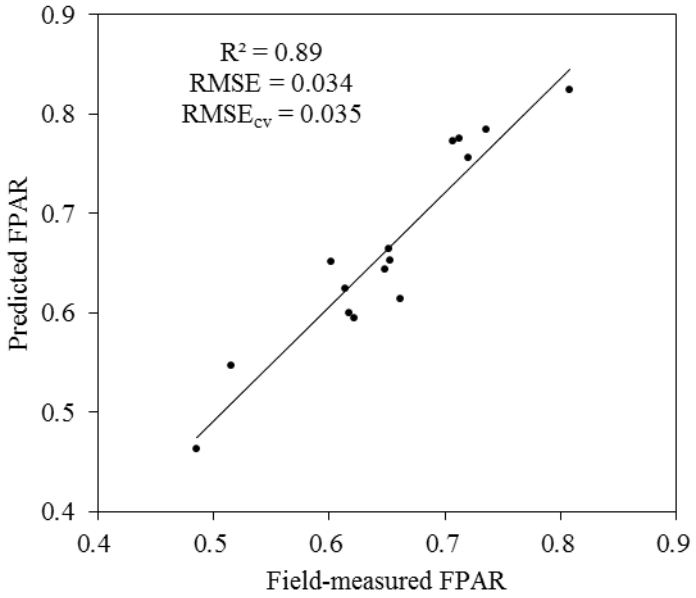

Fig. 4. Scatterplot of the intensity-based LiDAR-predicted FPAR and the field-measured FPAR and the corresponding linear regression (R2 = 0.89, RMSE = 0.034, p<0.001, n = 15).

4. Discussion

In this study, we explored the potential of airborne discrete-return LiDAR data in estimating FPAR of maize. Results show that airborne LiDAR data can be used to estimate FPAR accurately. However, LiDAR data acquisitions over large areas are extremely expensive and they become more expensive at higher sampling densities [57]. LiDAR and optical remotely sensed data can be considered complementary, as LiDAR can provide vertical structural information of canopy and optical data can reflect the spectral information of the ground cover [57]. Fusion of airborne LiDAR and multispectral or hyperspectral imagery has promising prospective for estimating FPAR at regional scales [58–60]. More effort is needed to study how to combine airborne LiDAR data and optical remotely sensed imagery to retrieve vegetation biophysical parameters (e.g., biomass and structure) [61, 62].

The FPAR estimation approach developed in this study can be applied to other sites. However, since the estimation model is empirical, it could not be directly used for different study areas and vegetation types, and LiDAR data must be analyzed and modeled according to actual situations to obtain the optimal FPAR estimation model suitable for the study area.

Thomas et al. [38] conducted spatial simulations of FPAR using a LiDAR-hyperspectral approach and found the strongest correlation between FPAR and mean LiDAR height. Here we also performed a linear regression analysis between mean LiDAR height and the field-measured FPAR and found that the maximum R^2 between FPAR and mean LiDAR height was 0.61 (RMSE = 0.062), which is lower than the LiDAR intensity-based estimation model developed in this study. Moreover, Thomas et al. [38] showed that the optimal cell size for estimating FPAR was 20 m in their study. However, our results indicated that 4.0 m radius plot size was the appropriate scale for estimating FPAR of maize. The difference between our results and Thomas et al's could be due to different vegetation types, study areas, and average LiDAR point density.

The FPAR retrieved from airborne LiDAR data in this study is only the instantaneous value. Daily PAR can be calculated through integrating instantaneous PAR from sunrise to sunset [63]. To date, vegetation LiDAR research has been largely empirical, focusing on strong relationships between LiDAR-derived metrics and vegetation height, LAI, FPAR, biomass, and volume [38]. Further research on developing some innovative physically based

#200050 - $15.00 USD Received 25 Oct 2013; revised 18 Feb 2014; accepted 19 Feb 2014; published 26 Feb 2014
(C) 2014 OSA

methods, e.g., radiative transfer models [59, 64], to estimate biophysical and biochemical parameter from airborne LiDAR is needed.

5. Conclusions

FPAR is an important input parameter for terrestrial ecosystem models. Although many studies have shown that LiDAR is a viable technique for estimating FPAR, the majority of these studies are forestry-oriented. The aim of this study was to investigate the feasibility of applying discrete-return small-footprint LiDAR data to estimate FPAR of maize. A method to retrieve FPAR from LiDAR data was proposed and applied to a maize field in northwest China. The canopy and ground returns were first separated from raw LiDAR point clouds. The canopy fractional cover (*fCover*) was estimated based on the ratio of the number of canopy laser returns (or intensity sums) to total returns (or intensities). FPAR estimation models of maize were established based on linear regression analysis between the field-measured FPAR and the LiDAR-derived *fCover*. Results show strong correlations between the LiDAR-derived *fCover* and the field-measured FPAR (R^2 = 0.90, RMSE = 0.032, p < 0.001). It was found that 4.0 m plot radius was the optimal scale for estimating FPAR. Accuracy in the estimated FPAR can be improved through normalizing the LiDAR intensity value based on a standard range and the incidence angle. It was also found that the LiDAR intensity-based FPAR estimation model had a higher accuracy compared to the LiDAR return-based FPAR model. The reliability of the LiDAR intensity-based FPAR model was assessed using the LOOCV procedure. Results show that the regression model is not overfitting. Finally, 15 independent field-measured FPARs (that were not used in the regression analysis) were used to evaluate accuracy of the LiDAR-predicted FPARs, and the coefficient of determination (R^2) is 0.89 and RMSE is 0.034.

Acknowledgments

This work was supported by the National Basic Research Program (973 Program) of China (2010CB951701), the National Natural Science Foundation of China (No. 41171279, No. 41371350); the 100 Talents Program of the Chinese Academy of Sciences and China Postdoctoral Science Foundation funded project (2013M530731). We thank three anonymous reviewers and associate editor Jean-Pierre Veran for many constructive comments.

#200050 - $15.00 USD Received 25 Oct 2013; revised 18 Feb 2014; accepted 19 Feb 2014; published 26 Feb 2014
(C) 2014 OSA

129.120.246.14 {ts '2018-08-25 14:28:04'}